ELSEVIER

Cement & Concrete Composites 24 (2002) 497–507

Cement & Concrete Composites

www.elsevier.com/locate/cemconcomp

Synthesis of punching failure in reinforced concrete

Ph. Menétrey *

Emch & Berger AG Bern, Gartenstrasse 1, 3001 Bern, Switzerland

Abstract

A synthesis of punching failure in reinforced concrete is given here. First, some recent experimental results are presented allowing one to show the difference between flexural and punching failure. Second, the punching failure mechanism is discussed based on results obtained with numerical simulations demonstrating among others the influence of the concrete tensile strength. Then, using these results, an analytical model is derived for punching load prediction. The model allows a unified treatment of slabs with various types of reinforcement. Finally, the prediction's capabilities are discussed using extended databases as well as special experimental results.

Keywords: Punching failure; Reinforced concrete; Experimental results; Numerical simulation; Analytical model; Shear reinforcement; Databank

1. Introduction

The punching failure of reinforced concrete slabs supported on columns occurs when a conical plug of concrete suddenly perforates the slab above the column. As this failure mechanism is brittle (occurring without any warning sign and with a high reduction of the load carrying capacity) various constructive methods were developed to avoid it. These include thickening of the slab, columns' capitals and different types of reinforcements such as flexural reinforcement, bent-bars, studs, stirrups, shear-heads and prestressed tendons. Consequently, the model for punching load prediction must treat all these different cases.

First, experimental results reported by Menétrey [17] are presented to show the difference between flexural and punching failure and to include the influence of the punching cone inclination. Second, results obtained by Menétrey et al. [20] with numerical simulations are presented to describe the punching failure mechanism and to extract the main parameters influencing punching failure.

Finally, the general model for punching load prediction developed by Menétrey [16,18] is presented. The punching strength is obtained by integrating the vertical components of the tensile stresses around the punching crack. The contribution of the reinforcements (flexural reinforcement, shear reinforcement and prestressed tendons) is taken into account similarly, by adding the vertical components of the tensile forces of each reinforcement crossing the punching crack. The resulting model is a unified and general model for punching load prediction. The prediction capabilities are discussed using the database developed by the *fib* task group 4.3 [8].

2. Experimental results

Punching failure based on experimental results was addressed by various authors, among others: Richart [27], Moe [22], Kinnunen and Nylander [13], Andersson [1], and Regan [26]. The focus here will be oriented toward the difference between flexural and punching failure. The experimental results obtained by Menétrey [17] on similar octagonal slabs (thickness: 120 mm; radius of support: 550 mm) differing only in their flexural reinforcements demonstrate this difference. Furthermore, the influence of the inclination of the punching crack is revealed.

These tests were performed by controlling the vertical displacement of the column (radius 120 mm) so that the response after peak load (descending branch) is captured. Four similar slabs are first considered with various cross-section of the bar (4–10 mm). Two slabs failed by flexural failure (slabs 9 and 10 with reinforcement

* Tel.: +41-31-385-61-11; fax: +41-31-385-61-12.

0958-9465/02/$ - see front matter
PII: S0958-9465(01)00066-X

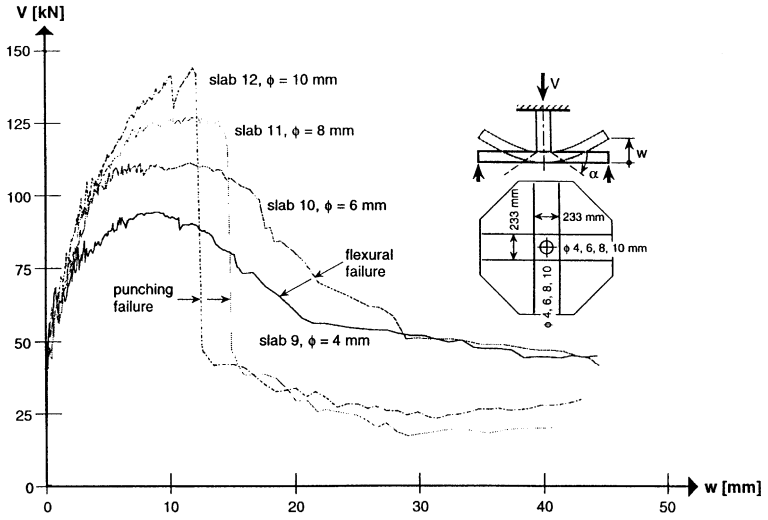

Fig. 1. Response curves for flexural and punching failure [17].

Fig. 2. Punching cone with different inclinations: 30°, 45°, and 60° [17].

$\varnothing = 4$ and 6 mm) characterized by a yield-line mechanism. Two slabs failed by punching (slabs 11 and 12 with reinforcement $\varnothing = 8$ and 10 mm) characterized by a punching cone. The load–displacement curves of the four slabs are shown in Fig. 1.

First, it is observed that the failure load is raised with increasing cross-section of the reinforcement. Then, the load–displacement curves illustrate that after the maximum load (peak load) has been reached, a flexural failure (slabs 9 and 10) is characterized by a smooth decrease of the carrying load with increasing displacement. In the opposite case, a punching failure results in a sudden decrease of the carrying load after the peak load has been reached (vertical branch of the response curves of slabs 11 and 12). These results clearly illustrate the difference between both failure mechanisms and also the reason why punching failure is so dangerous.

The geometry of the failure surface plays an important role, especially when the failure surface is forced into a shape different from that giving a pure punching failure as showed by Regan [26] (load close to the support) or by Azad et al. [2] (mechanical devices inside the slab). By controlling the size of ring reinforcement as established by Menétrey [17], the punching crack is generated at different inclinations: 30°, 45°, 60°, and 90° to the middle plane of the slab. A view of the resulting punching cone inclined at 30°, 45°, and 60° is presented in Fig. 2.

The load–displacement curves of these four slabs with different punching cone inclinations reveal a transition between punching and flexural failure which is controlled by the punching crack inclination α. An analytical expression was proposed by Menétrey [17] to determine the failure load in terms of the punching load F_{pun} and the flexural load F_{flex} so that

$$F_{\text{fail}} = F_{\text{pun}} + (F_{\text{flex}} - F_{\text{pun}}) \left\{ \sin \left[\frac{\pi}{\pi - 2\alpha_0} (\alpha - \alpha_0) \right] \right\}^{1/2}, \tag{1}$$

where α_0 is the inclination of the punching crack of a pure punching failure (see Section 4.2).

3. Numerical simulations

3.1. Description of the model

The numerical simulation of punching failure has recently be achieved by researchers including De Borst and Nauta [5], González et al. [11], Menétrey et al. [20] and Ozbolt et al. [23]. The simulation performed by Menétrey et al. [20] is detailed here. The model was developed to reproduce the different states of stress characterizing punching failure so that the triaxial failure criterion developed by Menétrey and Willam [21] was considered. The dilatancy observed experimentally is matched with a specific flow rule. The concrete cracking phenomenon is described with the smeared crack model using the strain-softening formulation. The fictitious crack model developed by Hillerborg et al. [12] is considered for which the reduction of the tensile stress σ_t is controlled by the crack opening w along the line of an exponential decohesion process. The fracture energy defined as the amount of energy absorbed per unit area in opening the crack from zero to the crack rupture opening w_r is

$$G_f = \int_0^{w_r} \sigma_t \, dw, \tag{2}$$

which is invariant with the finite element size. The simulation of localized failure like punching failure requires this dependence on the finite element size which plays the role of localization limiter. The connection between the brittleness of failure and the state of stress is reproduced by introducing a fictitious number of cracks.

3.2. Simulation of punching failure

The circular slab tested by Kinnunen and Nylander [13] and reinforced with ring reinforcement (denoted by IB15a) was simulated because of its perfect axially symmetric geometry. The punching failure simulation allows one to observe the cracking phenomenon in the vicinity of the column as illustrated in Fig. 3 for the three load steps preceding the failure.

It can be observed that the punching crack is initiated by coalescence of micro-cracks at the top of the slab. This coalescence phenomenon is justified experimentally by the tests of Regan [25] reporting that micro-cracks are formed across the slab thickness before failure occurs and Moe [22], who observed visually the formation of inclined cracks across the slab thickness before failure occurs. With increasing vertical displacement this inclined crack expands toward the corner of the slab–column intersection. At the same time, the other inclined micro-cracks are closing. At failure, the punching crack has reached the corner of the slab–column intersection. It can be observed that the punching crack orientation is close to the experimental one except at the top of the slab.

3.3. Parametric analysis

A parametric analysis is performed for a circular slab similar to that above but made with orthogonal reinforcement (modeled with ring and axisymmetric bar elements). The partial bond between concrete and steel is simulated by rigidly fastening the steel to the concrete only at the extremity of a fictitious fastening length. The purpose of this fictitious fastening length is to allow some cracks to grow and consequently others to close. This fictitious length is determined by analogy with the crack spacing observed during tensile tests on reinforced concrete specimens.

The concrete parameters such as the tensile and compressive strengths are known to be interrelated. However, for the following parametric analysis, they are considered independently (only one parameter is varied at a time) in order to determine their effects on the punching failure process. The influence of the uniaxial tensile strength and the fracture energy of concrete is investigated. The response curves shown in Fig. 4 clearly demonstrate the influence of both parameters.

However, the uniaxial concrete compressive strength has little influence on the punching failure as neither the cracking mechanism nor the response curve is modified for slabs with different uniaxial compressive strengths: $f_c = 22.5$, 28.1, and 33.7 MPa (when the tensile strength is held constant).

In contrast, Ozbolt et al. [23] reported little influence of the tensile and compressive concrete strength. This conclusion that punching failure is little influenced by the concrete strength is not justified experimentally. This can result from the assumption of a uniaxial stress strain response according to the micro-plane model for which the biaxial and triaxial concrete response are neglected.

The influence of the percentage of flexural reinforcement is studied by simulating slabs with different percentages: $\rho = 0.2\%$, 0.4%, 0.8%, 1.2%, 1.6%, and 2%. A similar cracking mechanism is observed for all these slabs. The corresponding response curves are presented in Fig. 5 in addition to the one of a flexural failure generated for a plain concrete slab. It can be observed that after a similar initial elastic behavior, the response of the slabs varies tremendously depending on the percentage of reinforcement. By increasing the percentage of reinforcement, the value of the punching load is

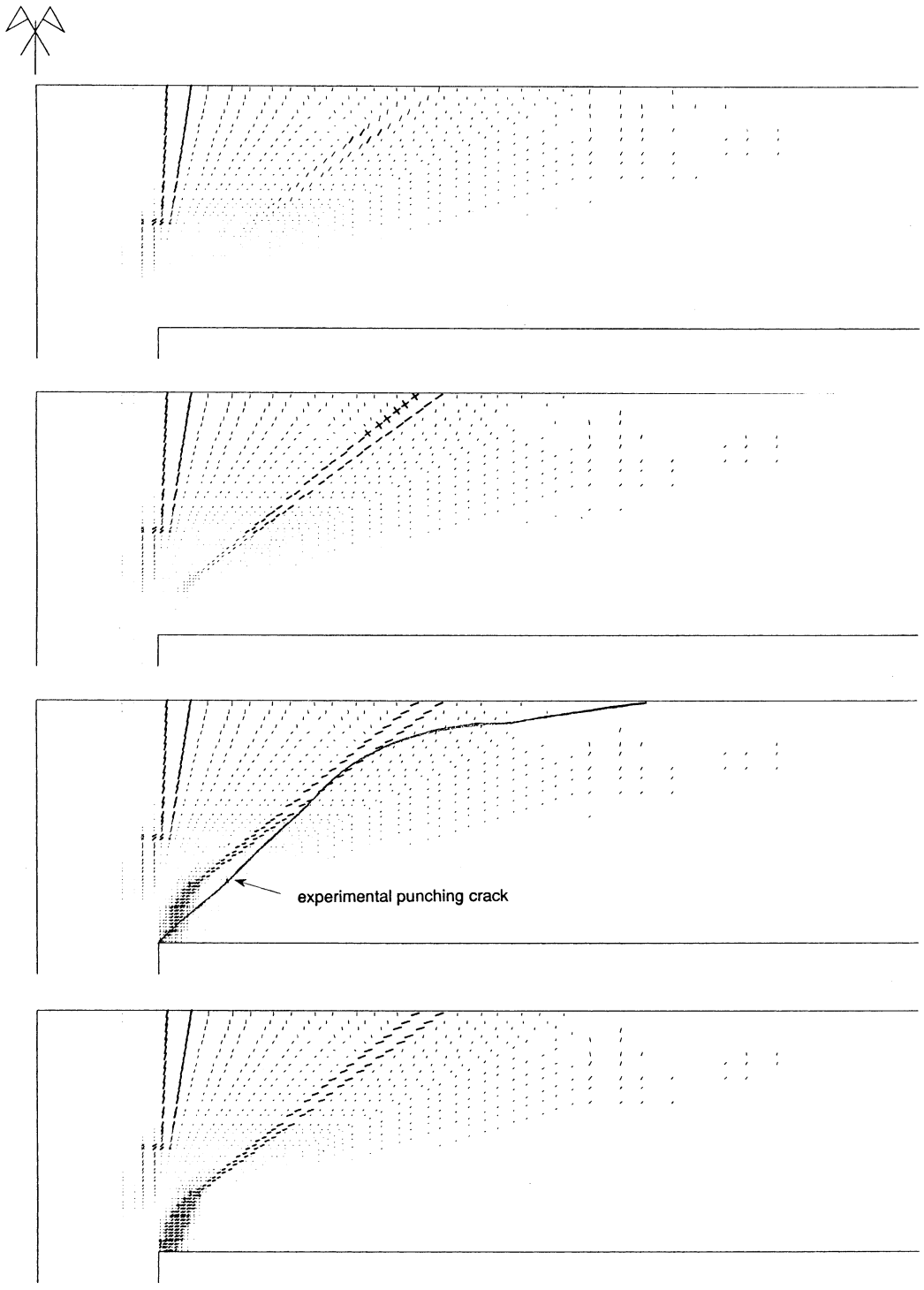

Fig. 3. Tangential cracks for ultimate vertical displacements: 3.1, 3.2, and 3.3 mm [20].

increased but the ductility is decreased. These results are comparable to the experimental results obtained by Elstner and Hognestad [9].

The size effect is investigated by simulating four slabs of different sizes (slab thickness: 75, 150, 300, 450 mm) but with a similar scaling factor which applies to the concrete geometry and the steel area. Except for these dimensions, the slabs have similar boundary conditions and material characteristics. The nominal shear stress at the failure load P_{failure} is computed as

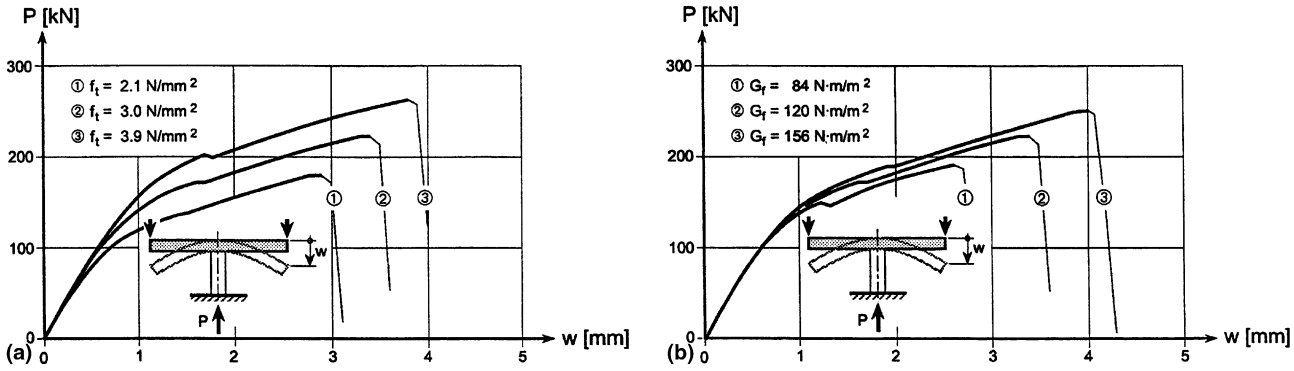

Fig. 4. Influence on the response curves of the concrete: (a) uniaxial tensile strength; (b) fracture energy [20].

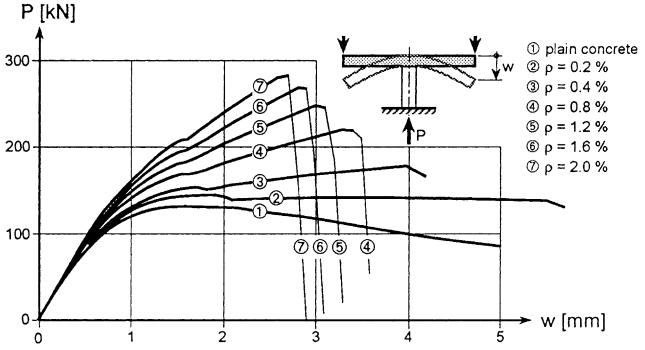

Fig. 5. Influence on the response curves of the percentage of reinforcement [20].

$$\tau_n = \frac{P_{failure}}{\pi(2r_s + d)d}, \tag{3}$$

where the radius of the column is denoted by r_s and d is the slab effective depth. As presented in Fig. 6 the nominal shear stress decreases with increasing thickness of the slab.

In assuming a constant fracture energy, Bažant [3] derived a size-effect law which was shown by Bažant and Cao [4] to describe the size effect in punching failure. This size-effect law is adjusted on the four slab simulations (without having the experimental scatter) following the RILEM Recommendations [24] by linear regression, which gives

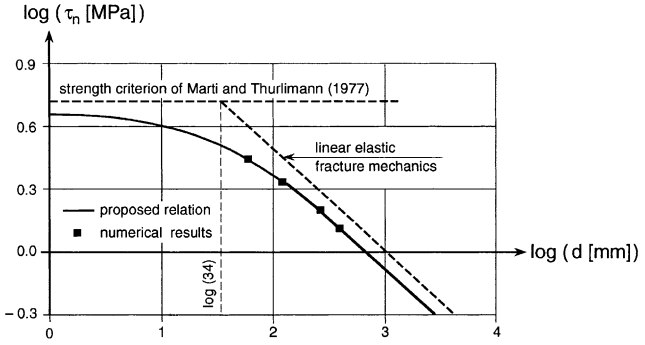

Fig. 6. Size-effect law derived from numerical simulations [20].

$$\tau_n = 1.55 f_t (1 + d/34)^{-1/2}, \tag{4}$$

where f_t is the uniaxial tensile strength of concrete. This relation is plotted in Fig. 6, in which the two asymptotes: horizontal one (strength criterion of Marti and Thürlimann [15]) and inclined one (linear elastic fracture mechanic) are distinguished.

4. Analytical model

4.1. Preliminaries

A synthesis of the analytical model developed by Menétrey [16] to compute the punching load of reinforced concrete slabs is presented here. The influence of the flexural capacity is linked to the punching shear capacity with the punching crack inclination as proposed by Menétrey [17] and presented here in Section 2. The expression is enhanced with the treatment of the contribution of the stirrups and shear reinforcements along the line of the work presented by Menétrey [18].

The proposed model is based on the observation that the punching load is influenced by the tensile stress in concrete along the inclined punching crack (key assumption of the model). Consequently, the punching load is predicted by integrating the vertical components of the tensile stresses around the punching crack. The contribution of the reinforcements is taken into account similarly, by adding the vertical components of the tensile forces of each reinforcement crossing the punching crack (flexural reinforcement, shear reinforcement, and prestressed tendons) so that the punching load of a general slab is expressed as

$$F_{pun} = F_{ct} + F_{dow} + F_{sw} + F_p, \tag{5}$$

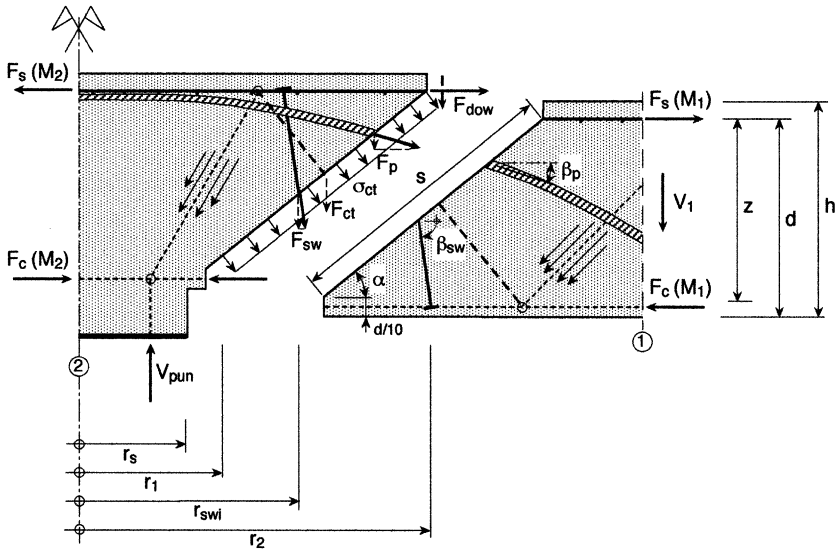

Fig. 7. Representation of the punching shear capacity [16].

where F_{ct} is the vertical component of the concrete tensile force obtained by integrating the vertical components of the tensile stresses in concrete, F_{dow} is the dowel-force contribution of the flexural reinforcement, F_{sw} is the vertical components of the forces in the studs, stirrups or bent-up bars which are well anchored and F_p is the vertical components of the forces in the tendons. The punching load of a slab is consequently computed in a unified manner by summation of all the vertical components of the tensile forces crossing the punching crack as illustrated in Fig. 7.

The punching failure is a sudden failure characterized by a rapid decrease of the load carrying capacity as shown in Fig. 1. However, the punching crack causing the punching failure is not formed suddenly, but is preceded by the formation of internal micro-cracks. Because the micro-crack formation is progressive, steel resistance is gradually activated and the force in the reinforcements can be added to the concrete tensile force as proposed by the general model in Eq. (5).

4.2. Link between punching and flexural capacity

The influence of the punching crack inclination was presented in Section 2 based on experimental results. It is shown that the punching crack inclination α allows one to link both flexural and punching failure loads and the analytical expression given in Eq. (1) is considered here. By assuming a punching crack inclination for pure punching failure of $\alpha_0 = 30°$ the general failure load of a slab can be expressed as

$$F_{fail} = F_{pun} + (F_{flex} - F_{pun})\left\{ \sin\left(\frac{3}{2}\alpha - 45°\right)\right\}^{1/2} \quad \text{with } 30° \leqslant \alpha \leqslant 90°. \tag{6}$$

It can be noted that $F_{fail} = F_{pun}$ for a punching crack inclination $\alpha = 30°$ and $F_{fail} = F_{flex}$ for $\alpha = 90°$. For design application, the flexural failure load F_{flex} can be determined with the yield-line theory as presented by Gesund and Kaushik [10]. For example, the ultimate load for the yield-line mechanism without cracking over the column is given by

$$F_{flex} = \frac{2\pi m_R}{1 - r_s/r_e}, \tag{7}$$

where m_R is the resistant bending moment and r_e the radius of the slab.

4.3. Concrete tensile force

The concrete tensile force is determined by integrating the vertical component σ_v of the tensile stresses σ_{ct} around the punching crack. The punching crack is assumed to be a truncated cone in shape comprised between two radii r_1 and r_2 as shown in Fig. 7 so that

$$r_1 = r_s + \frac{1}{10}\frac{d}{\tan\alpha} \quad \text{and} \quad r_2 = r_s + \frac{d}{\tan\alpha}, \tag{8}$$

where r_s is the radius of the column and α the punching crack inclination. The inclined length is expressed as

$$s = \sqrt{(r_2 - r_1)^2 + (0.9d)^2}. \tag{9}$$

Around the punching crack, a constant tensile stress distribution is assumed for simplicity. The analytical expression to compute the vertical component of the concrete tensile force is consequently expressed as follows:

$$F_{ct} = \pi(r_1 + r_2)s\sigma_v = \pi(r_1 + r_2)sf_t^{2/3}\xi\eta\mu. \tag{10}$$

The concrete tensile force is influenced by the tensile strength of concrete (shown in Fig. 4(a)) and the ana-

lytical relation given by $F_{ct} \propto f_t^{2/3}$ is considered. The influence of the percentage of reinforcement ρ on the tensile stresses was determined with the numerical simulations and is given by

$$\xi = \begin{cases} -0.1\rho^2 + 0.46\rho + 0.35, & 0 < \rho < 2\%, \\ 0.87, & \rho \geqslant 2\%, \end{cases} \quad (11)$$

where ρ is in percent. The size-effect law obtained numerically and presented in Fig. 6 is included in the developed analytical model with the parameter μ expressed as

$$\mu = 1.6(1 + d/d_a)^{-1/2} \quad \text{with } d > 3d_a, \quad (12)$$

where d_a is the maximum aggregate size. This size-effect law was derived for a constant ratio $h/r_s = 2$ where h is the slab thickness. However, as reported experimentally [6,29], the radius of the column or similarly the radius where the punching crack is initiated influences the size-effect law. This phenomenon was reproduced numerically and the following analytical expression was proposed:

$$\eta = \begin{cases} 0.1(r_s/h)^2 - 0.5(r_s/h) + 1.25, & 0 < r_s/h < 2.5, \\ 0.625, & r_s/h \geqslant 2.5. \end{cases} \quad (13)$$

This parameter is determinant to predict the punching load of slabs with shearhead or shear reinforcement for which the punching crack is located outside these reinforcements.

The influence of the fracture energy is not considered in the analytical model as this parameter does not greatly vary the punching load for standard concrete. However, for fiber concrete or high-strength concrete with extreme value of the fracture energy, the concrete tensile force contribution should consider the concrete fracture energy.

4.4. Dowel-effect contribution

The shear force which can be transferred by reinforcing bars crossing the punching crack is computed according to Menétrey [16] as

$$F_{dow} = \frac{1}{2} \sum^{bars} \varnothing_s^2 \sqrt{f_c f_s (1 - \zeta^2)} \sin\alpha, \quad (14)$$

where the summation is performed for all bars crossing the punching crack and $\varnothing_s$ is the diameter of the corresponding bars. A parabolic interaction is assumed between the axial force and the dowel force in the reinforcing bar which is expressed with the term $(1 - \zeta^2)$ where $\zeta = \sigma_s/f_s$ and σ_s is the axial tensile stress in the reinforcing bar which has a yield strength f_s. The tensile stress σ_s is obtained by projection of the force in the compressive strut $F_{pun}/\sin\alpha$ in the horizontal reinforcement which gives $F_{pun}/\tan\alpha$ and by dividing by the sum of the area of the reinforcing bars crossing the punching crack so that

$$\sigma_s = \frac{F_{pun}/\tan\alpha}{\sum^{bars} A_s}. \quad (15)$$

The dowel contribution in Eq. (14) is reduced with the term $\sin\alpha$ to take into account the angle between the flexural reinforcing bar and the punching crack (in a vertical plane). In Eq. (14), the factor $1/2$ gives the best approximation, because the reinforcing bars in the horizontal plane are not crossing the punching crack at a right angle.

4.5. Shear reinforcement contribution

Shear reinforcements such as studs, stirrups, bentbars or bolts are used in order to increase the failure load and to reduce the sudden decrease of the load carrying capacity. The computation of the failure load in such slabs should differentiate the following positions of the punching crack (illustrated in Fig. 8 for a slab with one row of studs):

1. A punching crack located in between the column face and the first row of shear reinforcement; the computation of the corresponding failure load must consider the interaction between the punching load F_{pun} and the flexural capacity F_{flex} in terms of the punching crack inclination α following Eq. (6). The punching crack inclination is: $\alpha_a = \arctan((r_{swi} - r_s)/d)$.

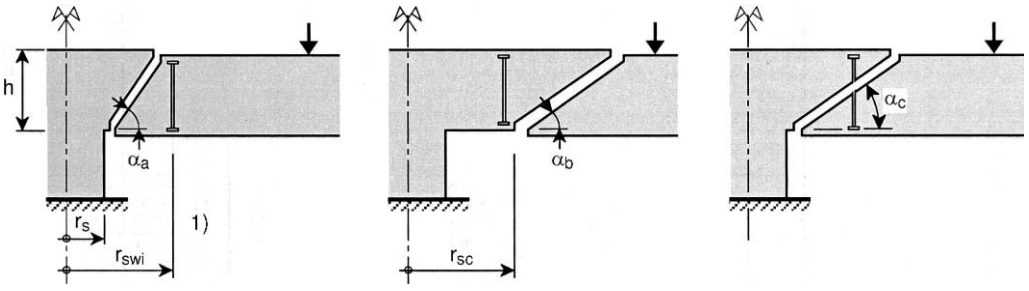

Fig. 8. Three positions of punching crack for slabs with one row of studs [18].

2. A punching crack which is initiated outside the last row of shear reinforcement; the punching shear capacity is computed similarly to the one of a normal reinforced concrete slab except that instead of the radius of the column r_s, the radius of punching crack initiation r_{sc} should be considered. The influence of this radius on the size effect is treated with the parameter η given in Eq. (13).
3. A punching crack which crosses the shear reinforcement.

The punching load corresponds to the minimum one of these different positions of the punching crack. The computation of the punching load for the third failure mechanism is addressed in the following.

The shear reinforcement contribution is influenced by it bond properties and two cases have to be distinguished: (1) shear reinforcements made with plain bars and anchorage denoted as *studs*, and (2) shear reinforcements made with high-bond bars denoted as *stirrups*. The contribution of the shear reinforcements to the punching load is computed by summing each contribution of reinforcement (in different rows, made with different types of reinforcement) crossing the punching crack.

The contribution of injected strengthening bolts (set after perforating the slab) is determined similarly to the contribution of studs or stirrups according to their bond properties. As a special case, for non-injected strengthening bolts, the concrete and the shear reinforcement contributions cannot be added because they do not interact as established by Menétrey and Brühwiler [19].

The contribution to the punching load of studs is considered for an axisymmetric reinforced concrete slab as illustrated in Fig. 9. This slab is reinforced with vertical studs well anchored at their extremities and made with plain bars characterized by a cross-section A_{sw} and a yield strength f_{sw}.

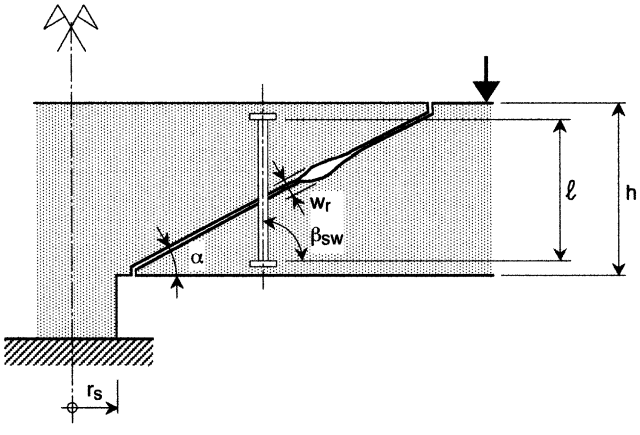

Fig. 9. Punching crack formation in slab with studs [18].

The failure mechanism for which the punching crack crosses the studs is initiated by micro-cracks. Due to micro-cracking the slab thickness increases, resulting in the loading of the studs. Consequently, the studs sustain a so-called displacement control loading for which the displacement corresponds to the summation of the micro-cracks' opening. This micro-crack formation is followed by the crack coalescence and the crack propagation which crosses the studs. Between the crack coalescence and the crack propagation, there is insignificant increase of load and no sudden change of the slab thickness as reported by Regan [25]. Therefore, the elongation of the studs at failure is expressed as illustrated in Fig. 9 by projection of the crack rupture opening w_r perpendicularly to the axis of the studs so that $\Delta l = w_r \cos\alpha$ ($\alpha =$ inclination of the punching crack). The studs' deformation is consequently $\epsilon_{sw} = \Delta l/l = w_r \cos\alpha/l$. Recalling the definition of the fracture energy in Eq. (2), the crack rupture opening is approached by

$$w_r \approx \frac{5G_f}{f_{sw}} \tag{16}$$

so that the maximum force is expressed as

$$F_{sw} = \sum^{studs} A_{sw}E_{sw}\frac{5G_f}{f_{sw}l\cos\alpha}\sin(\beta_{sw}) < A_{sw}f_{sw}\sin(\beta_{sw}) = F_{swy} \quad \text{for studs,} \tag{17}$$

where β_{sw} is the stud inclination. This force is limited by the yield strength of the studs up to the stud length $l_0 = w_r\cos\alpha E_{sw}/f_{sw}$. For higher stud length, the contribution to the punching load is reduced, reflecting a size effect inversely proportional to the stud length.

The same argument can be applied to determine the contribution of stirrups with high-bond bars. During micro-crack formation, the stirrups are crossed by various micro-cracks so that the tensile force inside the stirrups is distributed along the micro-cracked zone and is transmitted beyond this micro-crack zone to concrete by bond stresses. The tensile force in the stirrups is transmitted by bond stresses to concrete over the transmission length (defined as the length over which slip between steel and concrete occurs [7]). If this length is available, the yield strength of the stirrups is reached so that

$$F_{sw} = \sum^{stirrups} A_{sw}f_{sw}\sin(\beta_{sw}) = F_{swy} \quad \text{for stirrups,} \tag{18}$$

where β_{sw} is the stirrup inclination. If this length is not available, the carrying force in the stirrup is a function of the anchorage of the stirrup's extremity. Consequently, the anchorage of the stirrups has to be carefully set, specially in the top face of slabs (positive bending) and for short stirrups.

4.6. Prestressing tendons' contribution

The punching strength of a slab reinforced with inclined prestressing tendons is enhanced by adding the vertical components of the tendon forces. This vertical projection of the tendons' force is expressed as

$$F_{\mathrm{p}} = \sum^{\text{tendons}} A_{\mathrm{p}}\sigma_{\mathrm{p}}\sin(\beta_{\mathrm{p}}), \tag{19}$$

where the summation is performed for the prestressing tendons crossing the punching crack. A_{p} is the area of the prestressing tendons, σ_{p} is the tensile stress of the prestressing steel, and β_{p} is the inclination of the tendons at the intersection of the punching crack with the plane of the slab as shown in Fig. 7. The prestressing stress σ_{p} is considered and not the yield strength f_{p} of the tendons, because a shear failure does not allow large deformation, so that the yield strength cannot be reached. The influence of unbonded tendons is considered only with the vertical components of the tendons forces of Eq. (19). For bonded tendons, in addition to this contribution, the percentage of flexural reinforcement is increased by adding the percentage of reinforcement of the prestressing tendons in Eq. (11).

4.7. Comparison with experimental results

The predictions of the model are compared with the experimental data included in the database developed by the *fib* task group 4.3 [8]. For the prediction of the punching load of slabs without shear reinforcement only the terms F_{ct} and F_{dow} are activated according to Eq. (5). Due to the amount of tests and required data, some simplifications were made: (1) the punching crack inclination was assumed to be always 30°, (2) the data were taken as they were given without any special check, (3) some data like the aggregate size and the diameter of the flexural reinforcement were missing for various tests and in order to continue with a database with many tests, the data were completed and the aggregate size was assumed to be $d_{\mathrm{a}} = 20$ mm and the diameter of the flexural reinforcement was assumed to be $\varnothing_s = 10$ mm, and (4) no distinctions were made between circular and square slabs or columns (treated as circular ones). The comparison of the predicted and experimental results are shown in Fig. 10. The thick line shows the polynomial regression line which is very close to the ideal prediction line.

The prediction of the punching load for slabs with shear reinforcements was performed by adding the contribution F_{sw}. The differences between stirrups and studs as presented in Section 4.5 is not considered, because the concrete fracture energy necessary to express this difference was never reported experimentally. Therefore, Eq. (18) was considered, where the full strength of the shear reinforcement is activated. The prediction of the punching load for the three positions of the punching crack was performed. The punching load corresponds to the minimum value of the ones obtained with the three cracks and this value is plotted in Fig. 11. It can be seen that the dispersion is acceptable for the assumptions which were made. Furthermore, the prediction is not diffuse on the overall area, but is restricted to the area on the safety side.

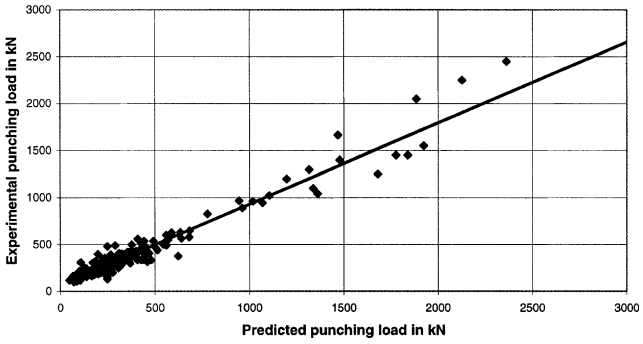

Fig. 10. Punching load prediction in slab without shear reinforcement.

The analytical contribution of the shear reinforcements is further controlled with detailed considerations of a few extreme experimental results which were not considered in the database [8]. The studs' contribution is controlled for two groups of tests summarized in Table 1 and the stirrups' contribution is controlled for one test.

The two slabs tested by Van der Voet et al. [29] are considered (abbreviated VdV): slab MV1 without shear reinforcement (punching load 375 kN) and slab MV6 (punching load 502 kN) for which the punching crack crosses 36 studs. It can be observed that the total yield strength of the studs ($F_{\mathrm{swy}} = 217$ kN) does not correspond to the increase of the punching load ($\Delta F_{\mathrm{exp}} = 127$ kN). However, by applying Eq. (17) with a crack opening $w_{\mathrm{r}} = 0.15$ mm (assumed) and a punching crack inclination $\alpha = 30°$ the contribution of the studs $F_{\mathrm{sw}} = 133$ kN is very close to experimental increase of the punching load.

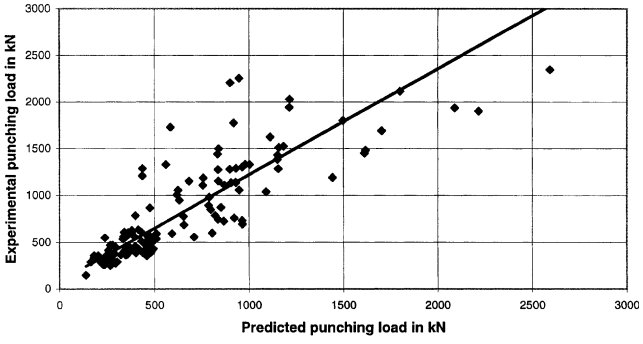

Fig. 11. Punching load prediction in slab with shear reinforcement.

Table 1
Comparison of experimental and predicted studs contributions

Slab	l (mm)	Studs Nb ∅ (mm)	f_{sw} (MPa)	F_{swy} (kN)	w_r (mm)	F_{sw} (kN)	ΔF_{exp} (kN)	$F_{sw}/\Delta F_{exp}$ (%)
VdV; MV6	137	36 ∅ 4.9	325	217	0.15	133	127	104
Tolf; S1.1s, S1.2s	105	16 ∅ 5	620	194	0.11	59	55	107
Tolf; S2.3s, S2.4s	210	8 ∅ 10	660	414	0.18	97	87	111

Similarly, the analytical computation of the studs contribution is controlled for two series of slabs tested by Tolf [28] for which stirrups with plain bars were used (considered here as stud). First, slabs S1.1–2 without shear reinforcement (punching load 205 kN) and S1.1–2s with shear reinforcements (punching load 260 kN) and second, slabs S2.3–4 without shear reinforcement (punching load 466 kN) and S2.3–4s with shear reinforcements (punching load 553 kN) are considered with a slab thickness of 120 mm respectively 240 mm. For both series of tests: (1) shear reinforcements are made with plain bars so that Eq. (17) developed for studs is applicable; (2) only the first row of studs is crossed by the punching crack; (3) the crack opening is computed by applying the method given by the CEB-FIP Model Code [7] with a mean compressive strength of 31 MPa and a maximal aggregate size of 16 mm for slabs S1 and 32 mm for slabs S2. As shown in Table 1 the analytical results are close to the experimental ones. Furthermore, by comparing the two test series, it can be observed that a simple strength criterion cannot be employed.

The influence of high-bond stirrups is controlled with the thick slab (730 mm) tested by Kinnunen et al. [14]. The reference slab S1 reaches a punching load of 4915 kN and slab S2 reinforced with high-bond stirrups reaches a punching load of 8320 kN so that the increase of punching strength due to the stirrups obtained experimentally is $\Delta F_{exp} = 3400$ kN. Only the first row of stirrups is crossed by the punching crack (72 stirrups of diameter 12 mm and yield strength $f_s = 428$ MPa). The stirrups' contribution reaches the yield strength $F_{sw} = F_{swy} = 3480$ kN, which is verified to be very close to the experimental contribution (102%).

5. Conclusion

A synthesis of punching failure in reinforced concrete has been presented here. Some recent experimental results were presented to show the difference between punching and flexural failure and the influence of the punching cone inclination.

Numerical simulations were presented to describe the punching failure mechanism and to extract the main parameters, among others the concrete tensile strength.

An analytical model to predict the punching failure load which is based on the integration of the vertical components of the tensile stresses around the punching crack has been derived. The strength of the reinforcement is treated in a unified way by adding the vertical components of the tensile forces in each type of reinforcement crossing the punching crack, so that the dowel force, the force in studs and stirrups, and the prestressing tendons contributions are taken into account. The predicted failure load is successfully compared with the experimental results available in database and also some special punching experiments.

References

[1] Andersson JL. Punching of concrete slabs with shear reinforcement. Transactions 212, Royal Institute of Technology, Stockholm, 1963.
[2] Azad AK, Baluch MH, Al-Mandil MY, Sharif AM, Kareem K. Loss of punching capacity of bridge deck slabs from crack damage. ACI Struct J 1993;90:37–41.
[3] Bažant ZP. Size effect in blunt fracture: concrete, rock, metal. J Eng Mech 1984;110(4):518–35.
[4] Bažant ZP, Cao Z. Size effect in punching shear failure of slabs. ACI Struct J 1987;84:44–53.
[5] De Borst R, Nauta P. Non-orthogonal cracks in a smeared finite element model. Eng Comput 1985;2:35–46.
[6] Corley WG, Hawkins NM. Shearhead reinforcement for slabs. ACI J 1968.
[7] Comité Euro-International du Béton. CEB-FIP model code, 1990. Bulletin d'information 195–196, Comité Euro-International du Béton, CH-1015 Lausanne.
[8] Fédération International du Béton. Punching of structural concrete slabs, 2001. Bulletin d'information xxx [to appear].
[9] Elstner RC, Hognestad E. Shearing strength of reinforced concrete slabs. J ACI 1956;28(1):29–58.
[10] Gesund H, Kaushik YP. Yield line analysis of punching failure in slabs. Publications 30-I, International Association for Bridges and Structural Engineering, 1970.
[11] González-Vidosa F, Kotsovos MD, Pavlović MN. Symmetrical punching of reinforced concrete slabs: an analytical investigation based on nonlinear finite element modeling. ACI Struct J 1988; 85(3):241–50.
[12] Hillerborg A, Modeer M, Petersson PE. Analysis of crack formation and crack growth in concrete by means of fracture

mechanics and finite element. Cem Concr Res US 1976;6:773–82.
[13] Kinnunen S, Nylander H. Punching of concrete slabs without shear reinforcement. Transactions 158, Royal Institute of Technology, Stockholm, 1960.
[14] Kinnunen S, Nylander HP, Tolf P. Plattjocklekens inverkan pa betongplattors hallfasthet vid genomstansning. Försök med rektangulära plattor. Bulletin 137, Institutionen för Byggnadsstatik Kungl, Tekniska Högskolan, Stockholm, 1980.
[15] Marti P, Thürlimann B. Fliessbedingung für Stahlbeton mit Berücksichtigung der Betonzugfestigkeit. Bericht 67, Institut für Baustatik und Konstruktion ETH Zürich, 1977.
[16] Menétrey Ph. Analytical computation of the punching strength of reinforced concrete. ACI Struct J 1996;93(5):503–11.
[17] Menétrey Ph. Relationship between flexural and punching failure. ACI Struct J 1998;95(4):412–9.
[18] Menétrey Ph. Punching in slabs with shear reinforcements: a tensile failure. In: Structural concrete – the bridge between people. fib Symposium, 1999; Prague.
[19] Menétrey Ph, Brühwiler E. Punching shear strengthening of reinforced concrete: experimental and analytical investigations. In: Structural faults and repair. Edinburgh; 1997. p. 451–8.
[20] Menétrey Ph, Walther R, Zimmermann Th, Willam KJ, Regan PE. Simulation of punching failure in reinforced-concrete structures. J Struct Eng: Struct Div ASCE 1997;123(5):652–9.
[21] Menétrey Ph, Willam KJ. A triaxial failure criterion for concrete and its generalization. ACI Struct J 1995;92(2):311–8.
[22] Moe J. Shearing strength of reinforced concrete slabs and footings under concentrated loads. Bulletin D47, Portland Cement Association, 1961.
[23] Ozbolt J, Vocke H, Eligehausen R. Three-dimensional numerical analysis of punching failure. In: Silfwerbrand J, Hassanzadeh G, editors. International Workshop on Punching Shear Capacity of RC Slabs. Stockholm: Royal Institute of Technology; 2000. p. 65–73.
[24] RILEM Draft Recommendations. Size–effect method for determining fracture energy and process zone size of concrete, 1990. Materials and Structures, 23.
[25] Regan PE. Punching shear in prestressed concrete slab bridges. Technical Report, Engineering Structures Research Group, Polytechnic of Central London, 1983.
[26] Regan PE. The dependence of punching resistance upon the geometry of the failure surface. Mag Concr Res 1984;36(126):3–8.
[27] Richart FE. Reinforced concrete walls and column footings, parts 1 and 2. J ACI 1948;20(2–3):97–127 [see also 237–60].
[28] Tolf P. Plattjocklekens inverkan pa betongplattors hallfasthet vid genomstansning. Försök med cirkulära plattor. Bulletin 146, Institutionen för Byggnadsstatik Kungl, Tekniska Högskolan, Stockholm, 1988.
[29] Van Der Voet AF, Dilger WH, Ghali A. Concrete flat plates with well-anchored shear reinforcement elements. Can J Civ Eng 1982;9(1):107–14.